Supporting Information

Supramolecular fluorescence array sensor for toxic heavy metal ions detection in environmental water and rice seedling extracts

Ru-Pei Yang[a], Shu-Zhen Huang[a], Kai-Ni Wei[a], Qing Tang[c], Zhu Tao[a], Ying Huang[a,b, *] An-Ting Zhao[a**]

[a] *Key Laboratory of Macrocyclic and Supramolecular Chemistry of Guizhou Province, Guizhou University, Guiyang 550025, China.*

[b] *The Engineering and Research Center for Southwest Bio-Pharmaceutical Resources of National Education Ministry of China, Guizhou University, Guiyang 550025, China*

[c] *Department College of Tobacco Science, Guizhou University, Guiyang 550025, China*

Correponding e-mail: yinghung128@163.com

Contents

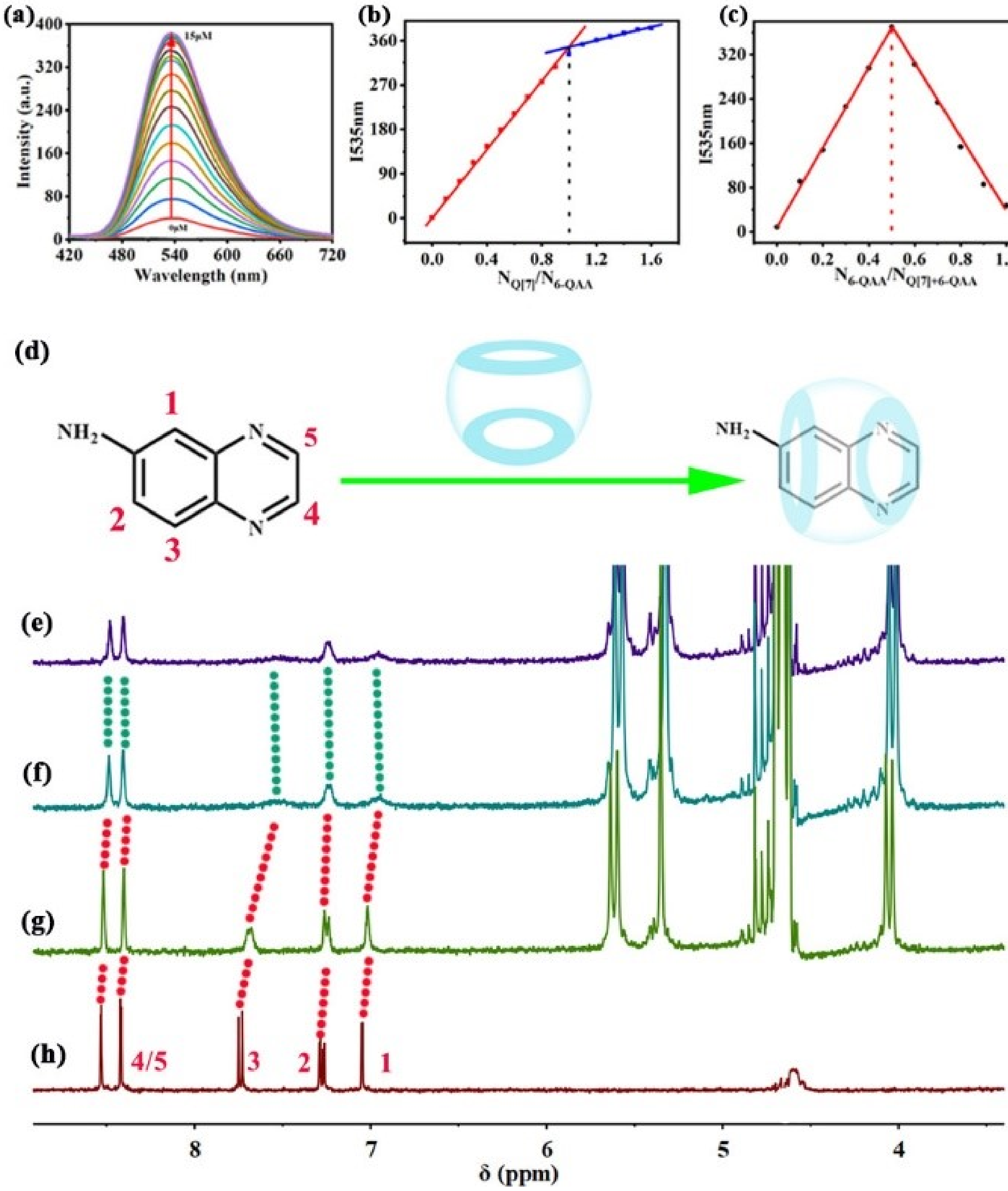
(a)
Intensity (a.u.)
Wavelength (nm)
15μM
0μM
(b)
I535nm
N_Q[7]/N_6-QAA
(c)
I535nm
N_6-QAA/N_Q[7]+6-QAA
(d)
NH2
1
2
3
4
5
N
(e)
(f)
(g)
(h)
4/5
3
2
1
δ (ppm)

Fig.S1 (a) Changes of fluorescence spectra of 10μM 6-QAA solution with the increase of Q[7] solution, (b) Scatter diagram of fluorescence action of 10μM 6-QAA solution with the increase of Q [7] solution, (c) Job diagram of $N_{6\text{-QAA}}$ /$N_{Q[7] + N6\text{-QAA}}$, (d) the possible interaction modes and ^{1}H NMR titration spectra of 6-QAA recorded upon the addition of Q[7], respectively (e) 6-QAA / Q[7](1:1.5), (f) 6-QAA / Q[7] (1:1), (g) 6-QAA / Q[7] (1:0.5), (h) 6-QAA.

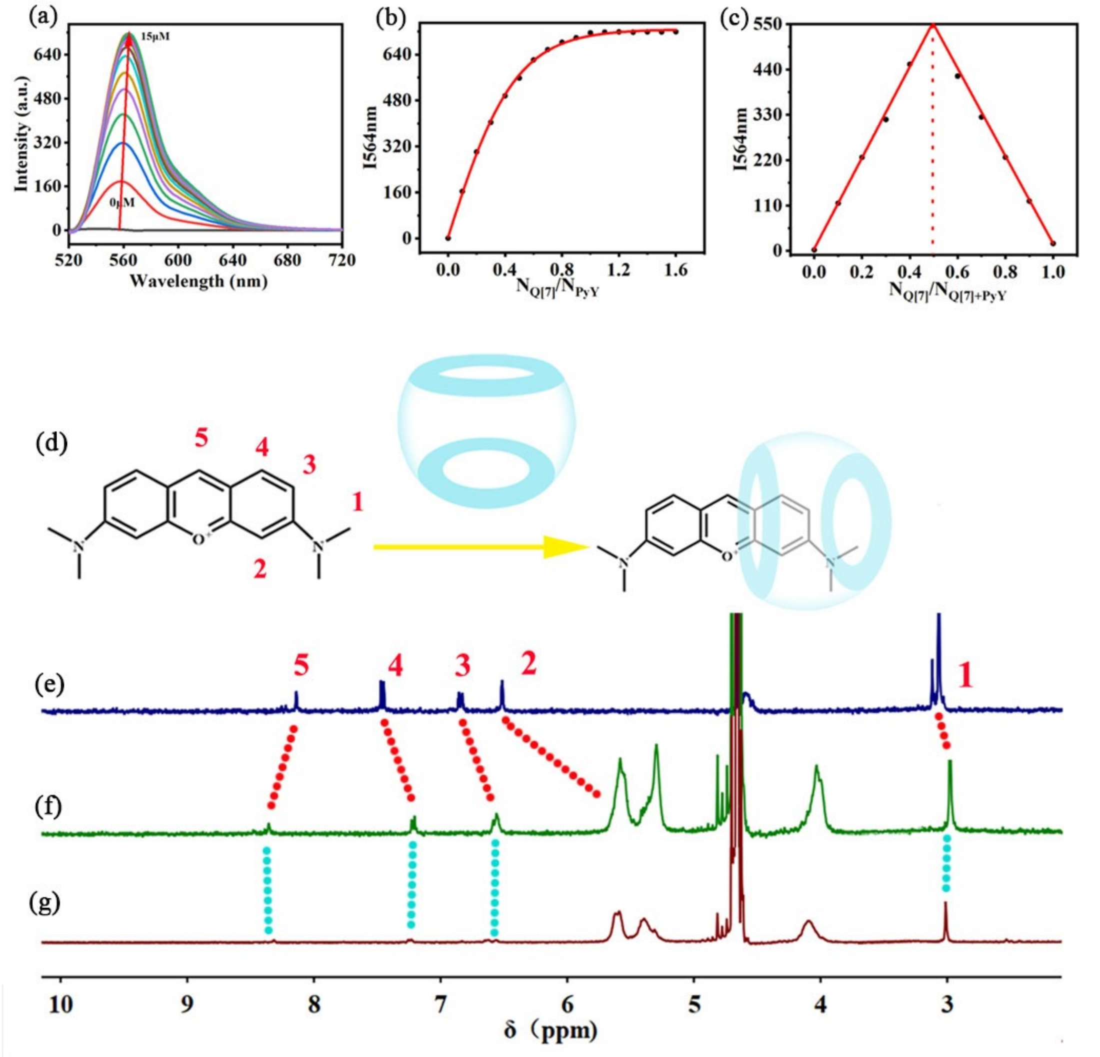

Fig.S2 (a) The fluorescence spectra of 10μM PyY solution changed with the increase of Q[7] solution, (b) The fluorescence interaction scatter diagram of 10μM PyY solution increased with the increase of Q[7] solution, (c) The Job diagram of N_{PyY} / $N_{Q[7] + PyY}$, (d) the possible interaction modes and ^{1}H NMR titration spectra of PyY recorded upon the addition of Q[7], (c) respectively (e) PyY , (f) PyY / Q[7](1:0.5), (g) PyY / Q[7](1:1).

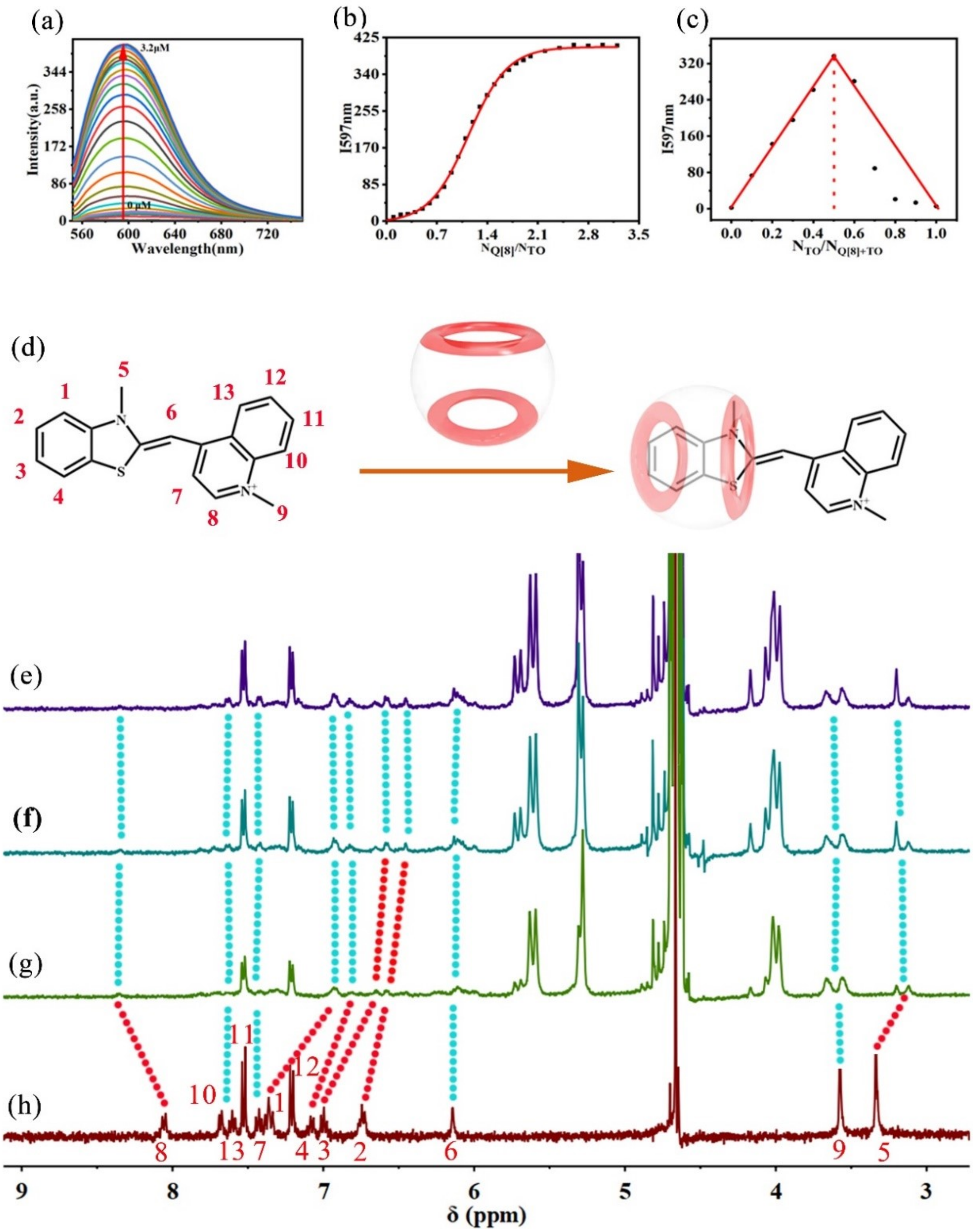

Fig.S3 (a) The change of fluorescence spectra of 10μMTO solution with the increase of Q[8] solution, (b) The fluorescence interaction scatter diagram of 10μMTO solution with the increase of Q[8] solution, (c) The Job diagram of N_{TO} / $N_{Q[8] + TO}$, (d) the possible interaction modes and ^{1}H NMR titration spectra of TO recorded upon the addition of Q[8](c), respectively (e) TO / Q[8](1:1.5), (f) TO / Q[8](1:1), (g) TO / Q[8](1:0.5), (h) TO.

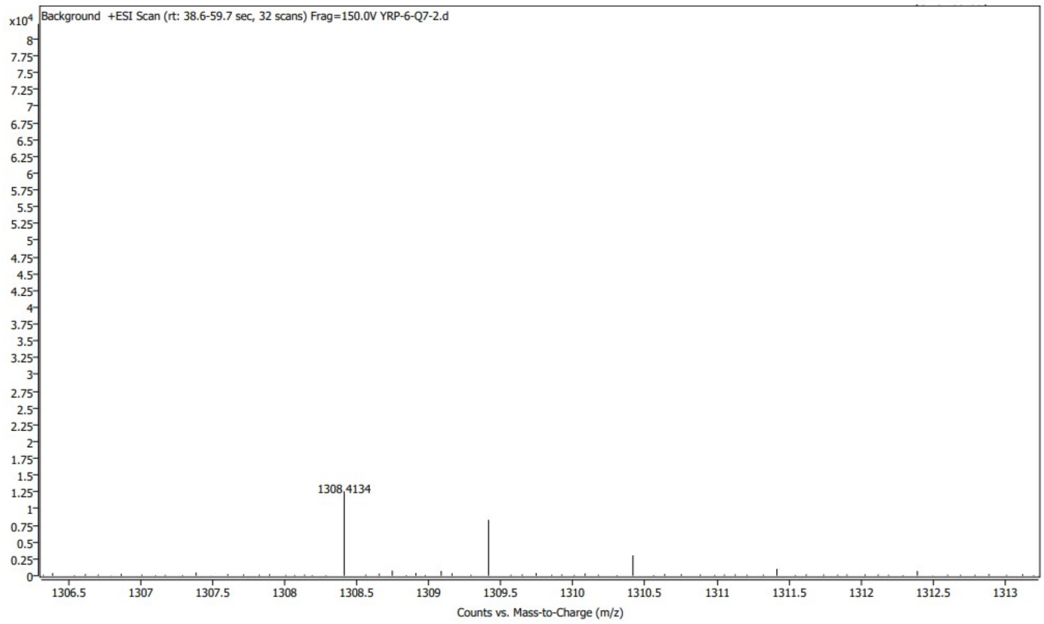

Fig.S4 The Mass spectrum of 6-QAA@Q[7], $[M+H^+]$=1308.41.

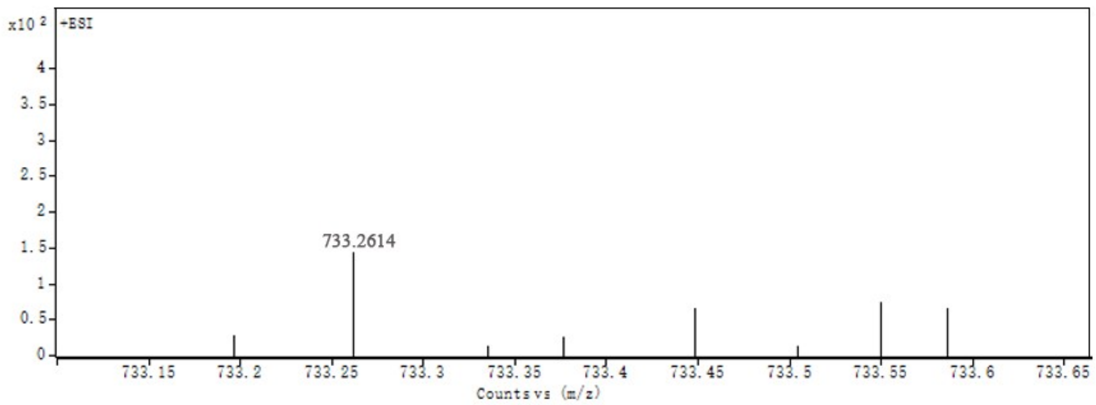

Fig.S5 The Mass spectrum of PyY@Q[7], $[M+2H^+]$=733.26

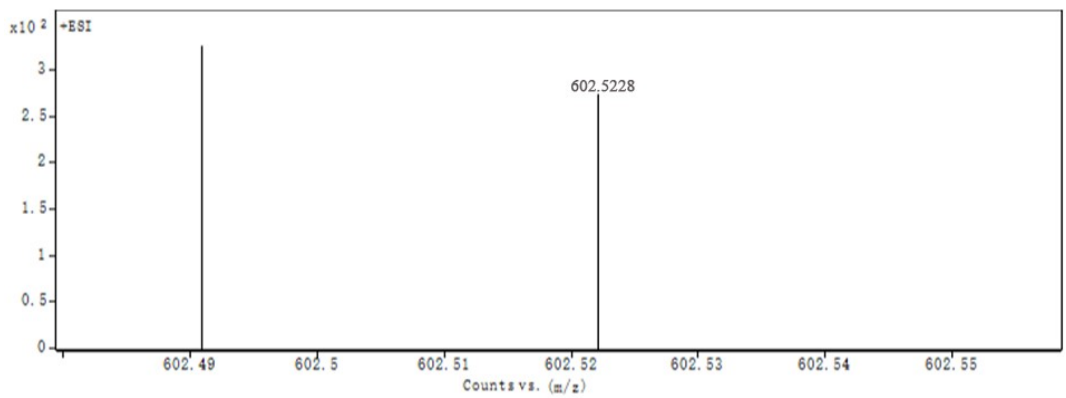

Fig.S6 The Mass spectrum of TO@Q[7], $[M+3H^+]$=602.52

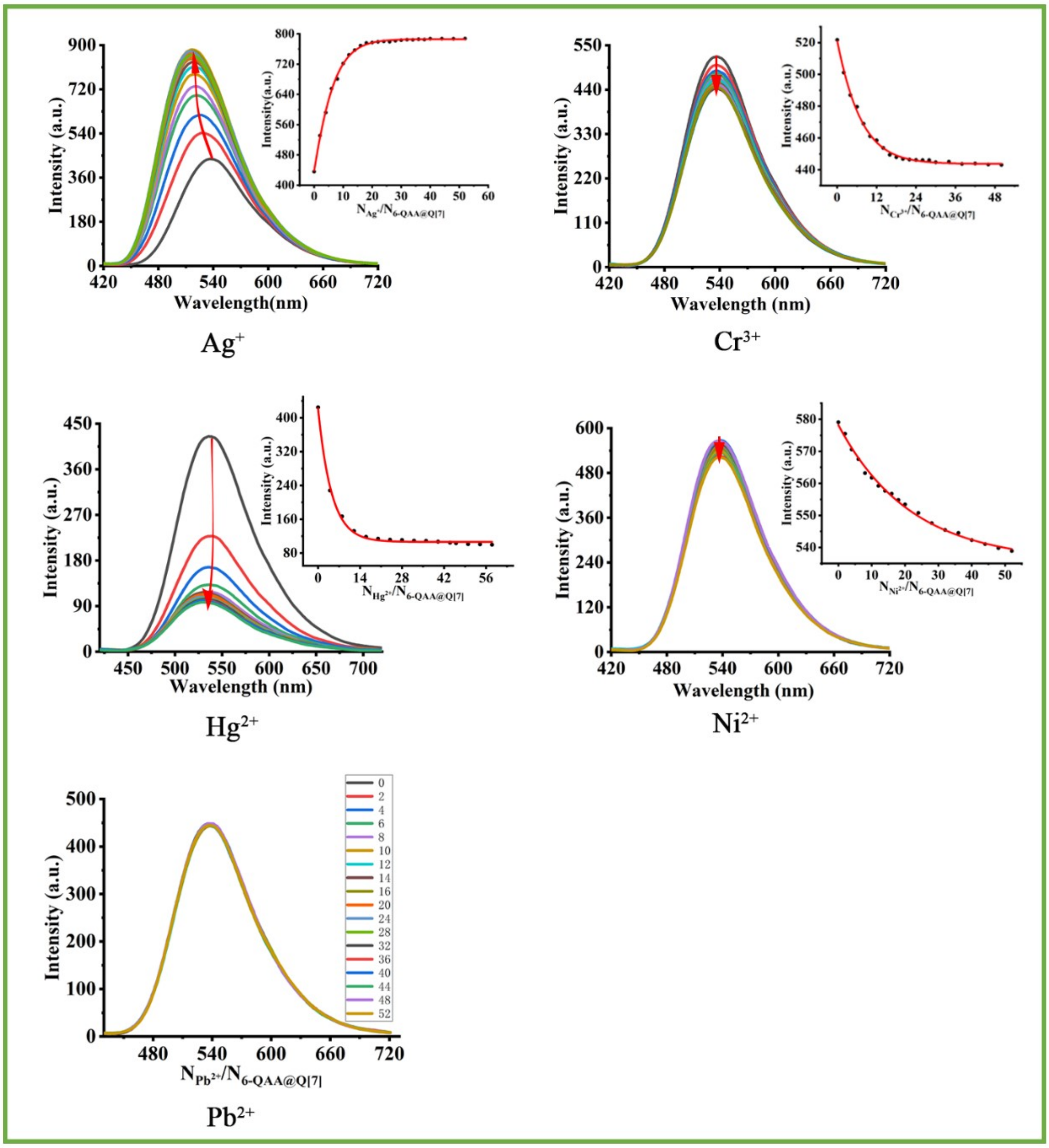

Fig.S7 The fluorescence intensity of 6-QAA@Q[7] and NM^{n+} / $N_{6\text{-}QAA@Q[7]}$ change with increasing concentrations of different metal ions (Ag^+, Cr^{3+}, Hg^{2+}, Ni^{2+}, Pb^{2+}

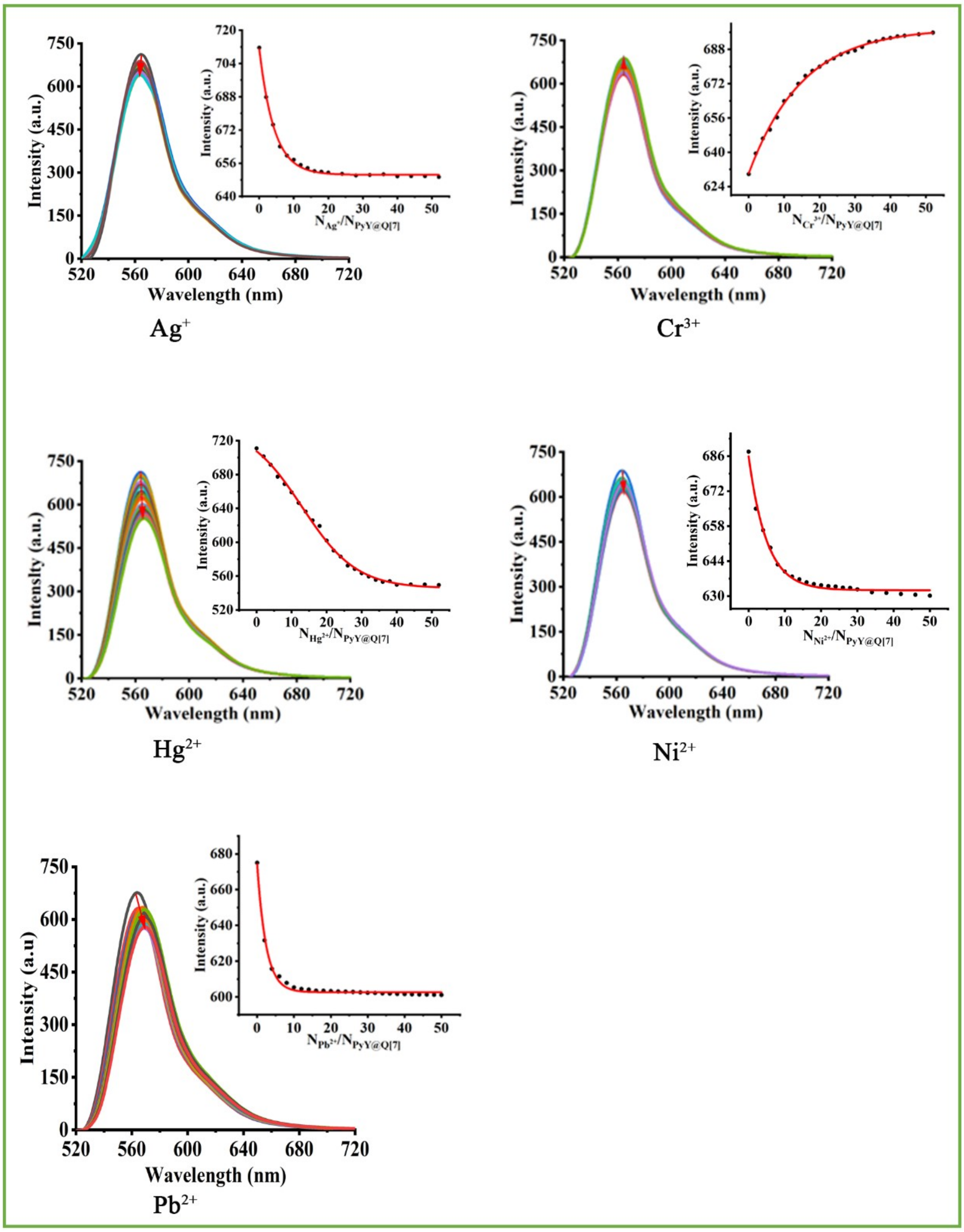

Fig.S8. Changes in fluorescence intensity of PyY@Q[7] and $N_{M^{n+}}$ / $N_{PyY@Q[7]}$ with increasing concentrations of different metal ions (Ag^{+}, Cr^{3+}, Hg^{2+}, Ni^{2+}, Pb^{2+})

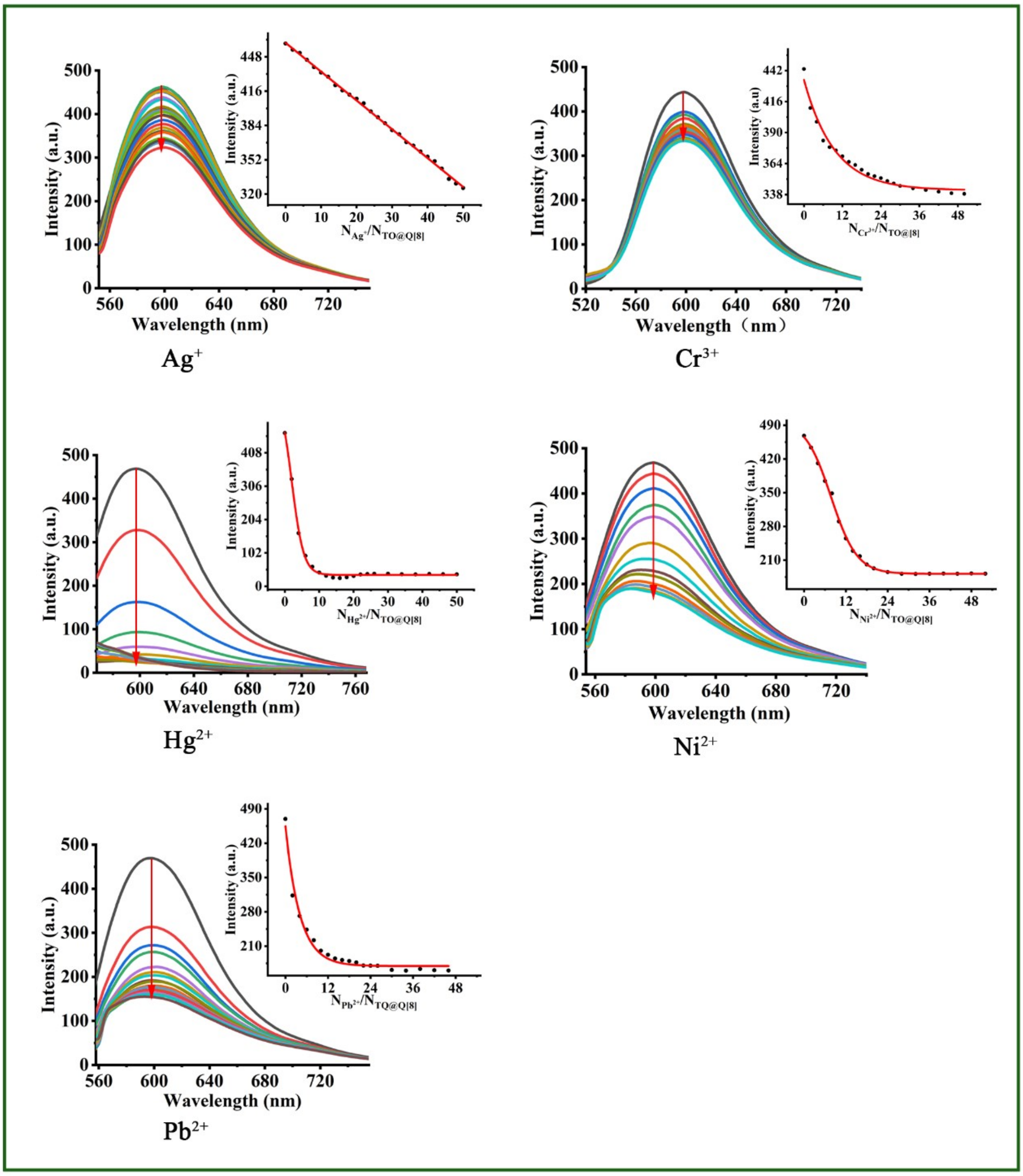

Fig.S9 Changes in the fluorescence intensity of TO@Q[8] and N_{M}^{n+} / $N_{TO@Q[8]}$ with increasing concentrations of different metal ions (Ag+, Cr^{3+}, Hg^{2+}, Ni^{2+}, Pb^{2+}).

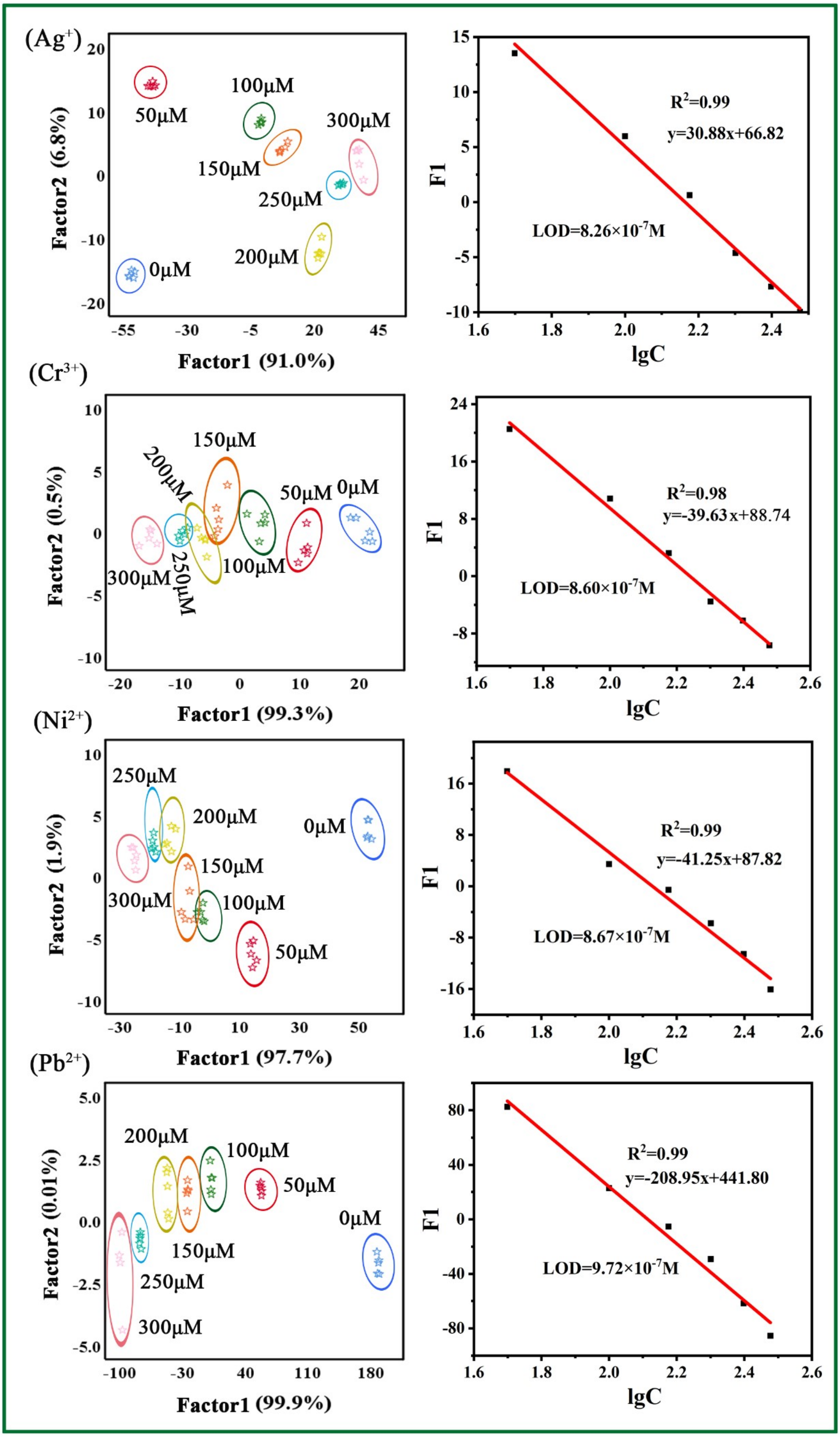
(Ag+)
50μM
100μM
300μM
150μM
250μM
200μM
0μM
Factor2 (6.8%)
Factor1 (91.0%)
R2=0.99
y=30.88x+66.82
LOD=8.26×10-7M
F1
lgC
(Cr3+)
150μM
200μM
50μM
0μM
300μM
250μM
100μM
Factor2 (0.5%)
Factor1 (99.3%)
R2=0.98
y=-39.63x+88.74
LOD=8.60×10-7M
F1
lgC
(Ni2+)
250μM
200μM
0μM
150μM
300μM
100μM
50μM
Factor2 (1.9%)
Factor1 (97.7%)
R2=0.99
y=-41.25x+87.82
LOD=8.67×10-7M
F1
lgC
(Pb2+)
200μM
100μM
50μM
0μM
150μM
250μM
300μM
Factor2 (0.01%)
Factor1 (99.9%)
R2=0.99
y=-208.95x+441.80
LOD=9.72×10-7M
F1
lgC

Figure. S10. the LDA score and linear relationship diagram of the array sensor for different concentrations of Ag^{+}, Cr^{3+}, Ni^{2+}, $Pb^{2+.}$

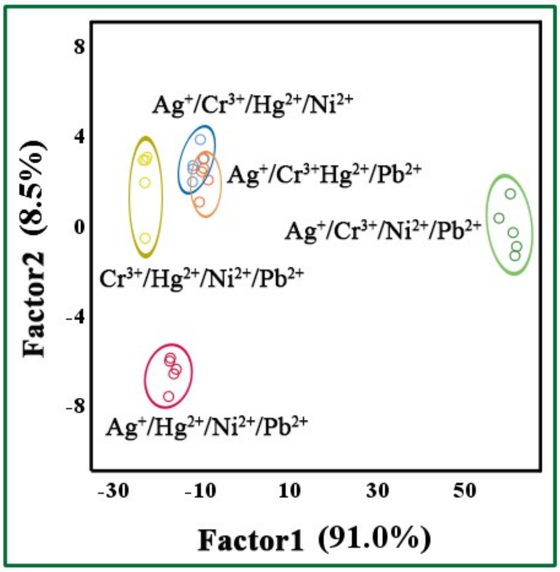

Figue. S11. Typical score plot of LDA response pattern of quaternary mixture

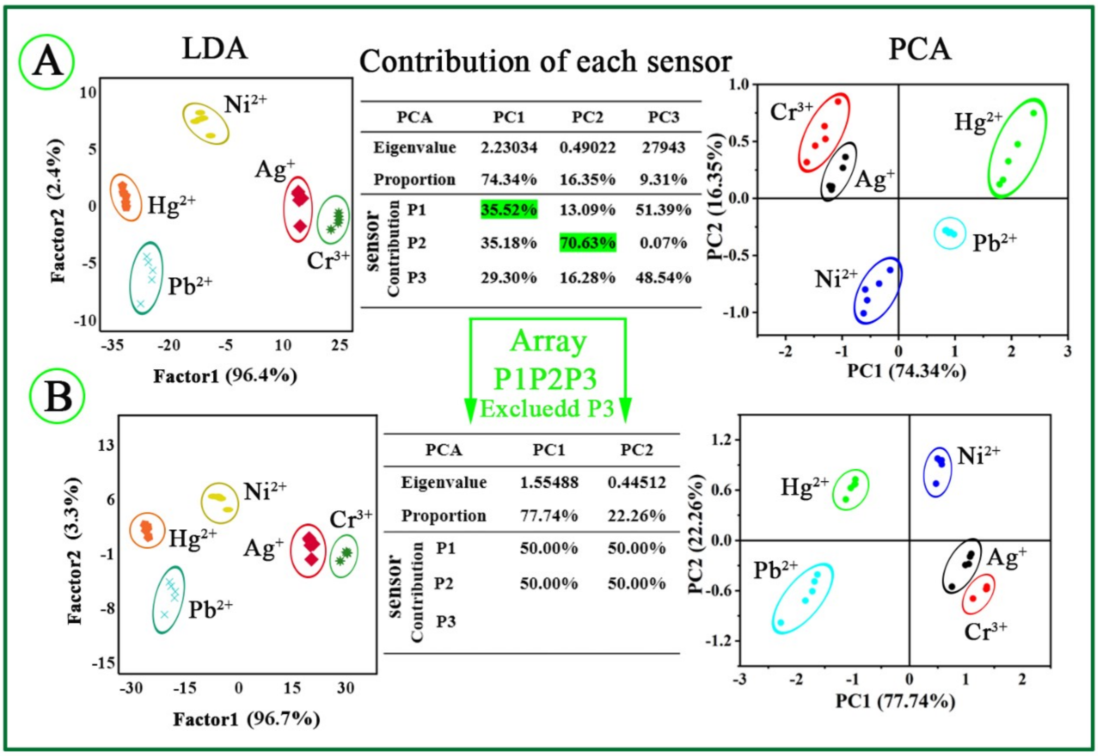

Fig. S12. (A) PCA showed the main contribution of array sensors (P1, P2, P3) to lake water samples (P1, P2, P3). (B) PCA shows the main contribution of sensors (P1 and P2).

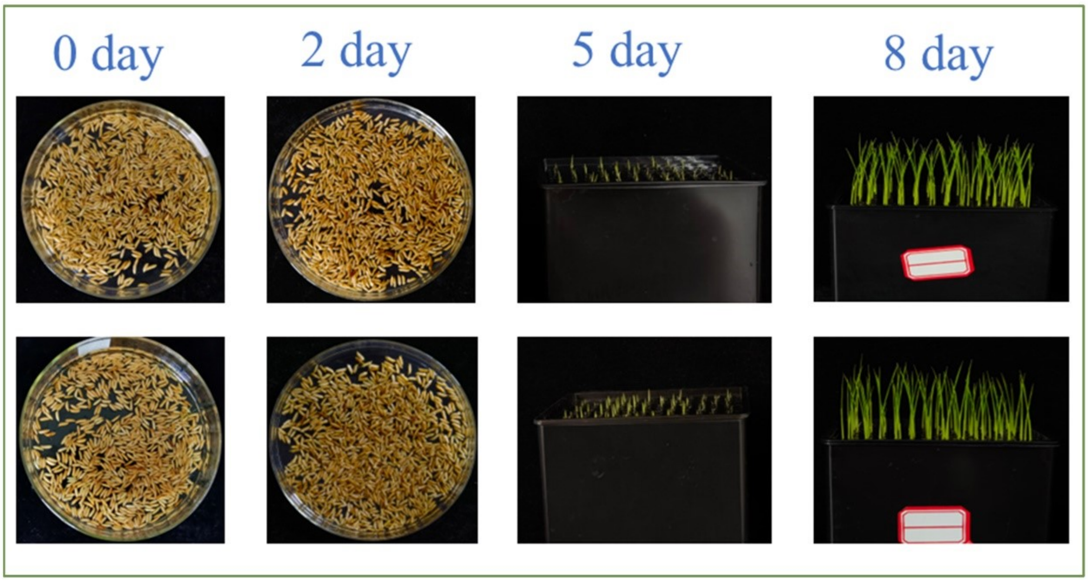

Fig. S13. Rice seeds before treatment and nutrient solution culture process.

(a)

Hg^{2+}(mg/kg)	A	ρ
0	0	-0.0118
0.05	38.1252	0.0414
0.1	81.5414	0.1020
0.2	152.9355	0.2016
0.5	375.3743	0.5118
1	736.7825	1.0160
2	1434.2842	1.9899

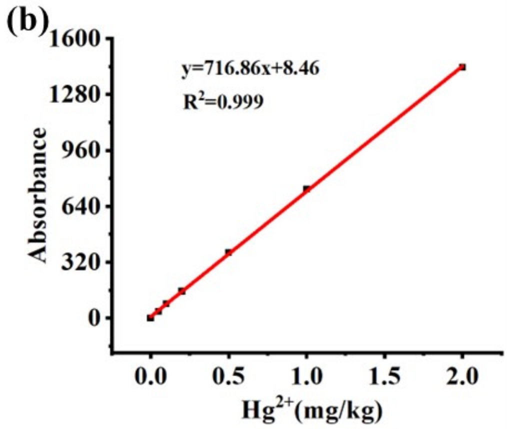

Figure. S14. (a) Hg standard curve data, (b) Hg standard curve graph. The 0.1000 g rice sample was ground and diluted to 100 ml, and 5 mL was diluted to 500 mL for detection. The measured A = 1282.67 was within the standard curve range of Hg, indicating that Hg^{2+} was absorbed in the extract.

Table S1 array sensor for five different metal ions to produce fluorescence response mode training matrix classification (500µM metal, 10µM ultrapure water sensor).

Metal			Predictive classification					
			Ag^{+}	Cr^{3+}	Hg^{2+}	Ni^{2+}	Pb^{2+}	total
Original	count	Ag^{+}	5	0	0	0	0	5
		Cr^{3+}	0	5	0	0	0	5
		Hg^{2+}	0	0	5	0	0	5
		Ni^{2+}	0	0	0	5	0	5
		Pb^{2+}	0	0	0	0	5	5
Cross-validated	count	Ag^{+}	5	0	0	0	0	5
		Cr^{3+}	0	5	0	0	0	5
		Hg^{2+}	0	0	5	0	0	5
		Ni^{2+}	0	0	0	5	0	5
		Pb^{2+}	0	0	0	0	5	5

Table S2 Sensor array for different Hg^{2+} concentration of fluorescence response mode training matrix classification.

Hg^{2+}(µM)			Predictive classification								
			0	50	100	150	200	230	250	300	total
Original	count	0	5	0	0	0	0	0	0	0	5
		50	0	5	0	0	0	0	0	0	5
		100	0	0	5	0	0	0	0	0	5
		150	0	0	0	5	0	0	0	0	5
		200	0	0	0	0	5	0	0	0	5
		230	0	0	0	0	0	5	0	0	5
		250	0	0	0	0	0	0	5	0	5

		300	0	0	0	0	0	0	0	5	5
Cross-validated	count	0	5	0	0	0	0	0	0	0	5
		50	0	5	0	0	0	0	0	0	5
		100	0	0	5	0	0	0	0	0	5
		150	0	0	0	5	0	0	0	0	5
		200	0	0	0	0	5	0	0	0	5
		230	0	0	0	0	0	4	1	0	5
		250	0	0	0	0	0	0	5	0	5
		300	0	0	0	0	0	0	0	0	5

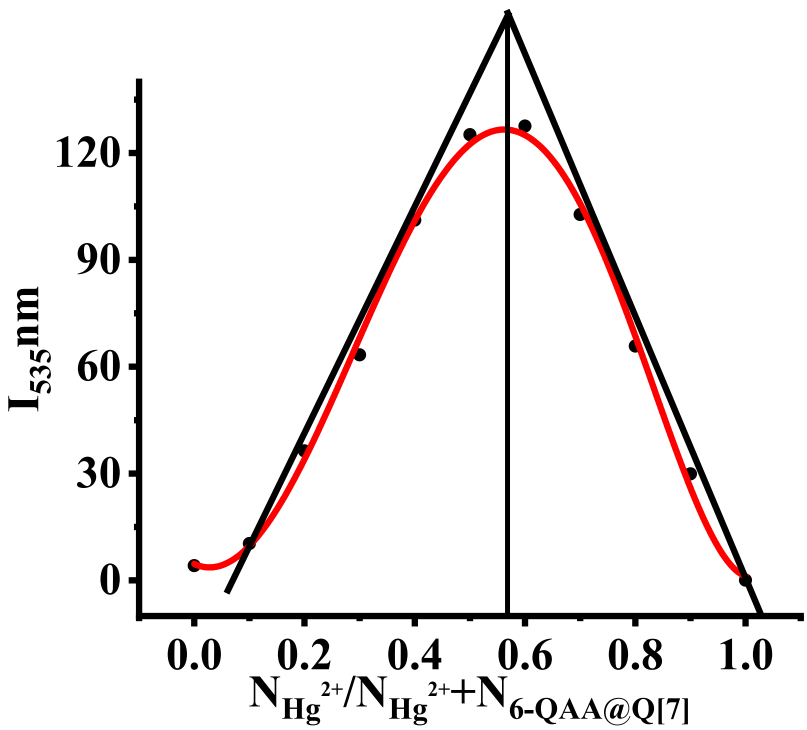

Fig S15 Job's plot obtained by continuous variation of the mole fraction of 6-QAA@Q[7] and Hg^{2+}

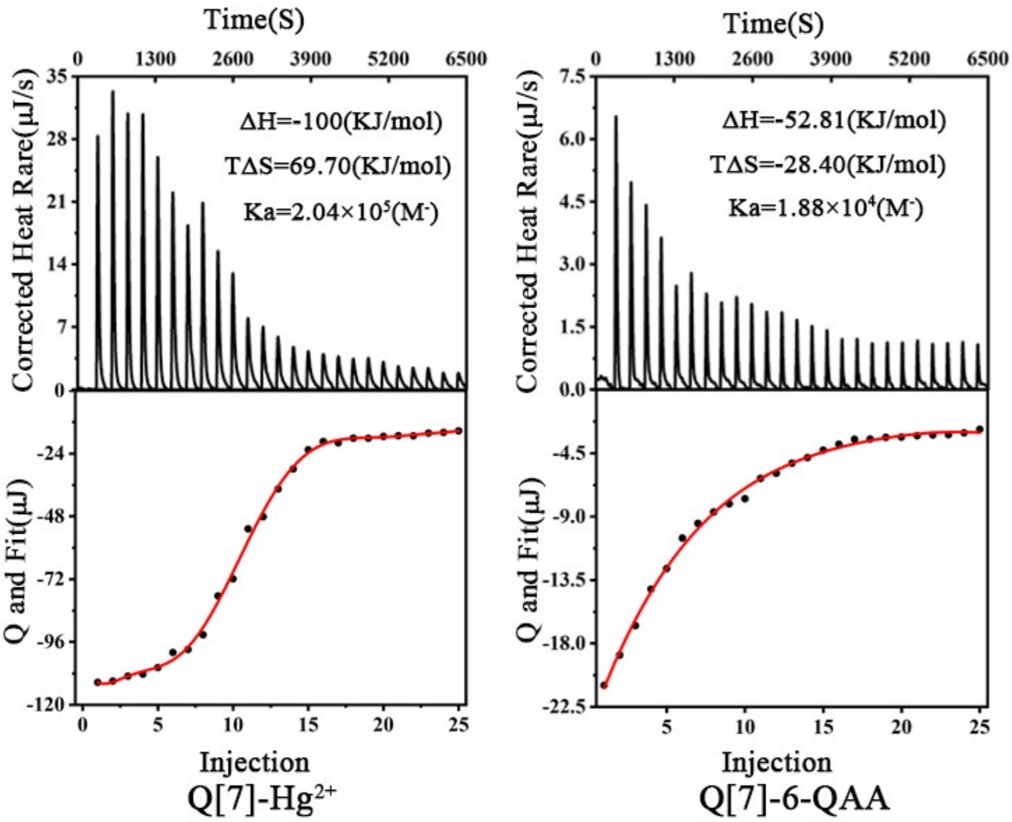

Fig S16 Isothermal titration calorimetry of 6-QAA and Hg^{2+} with Q[7] and related thermodynamic parameters.